ELSEVIER

Ultrasonics 40 (2002) 531–535

Ultrasonics

www.elsevier.com/locate/ultras

Contrast enhancement of ultrasonic imaging of internal stresses in materials

Michal Landa *, Jiří Plešek

Institute of Thermomechanics, Czech Academy of Sciences, Dolejškova 5, 182 00 Praha 8, Czech Republic

Abstract

The ultrasonic methods, which detect applied or residual stress in materials, are based on nonlinear interaction of a small dynamic disturbance (acoustic waves) with the pre-deformed state of the solid. This weak phenomenon (acoustoelasticity) leads to a dependence of acoustic wave velocities on the initial stress, and a stress-induced anisotropy in the acoustical properties of the material. In anisotropic media, the transversal wave velocity depends on its polarization. The amplitude of the conical polarized shear wave, propagating through a plate specimen, is sensitive to pre-stress due to acoustoelastic birefringence. The resulting scan image is created by variations of the amplitude. The previous description is a basic principle of the approach used for stress mapping in Al-alloys by time-resolved acoustic microscopy. Disk specimens with central stress concentrators are loaded step by step. The acoustic scans are created during each loading step. Thermal stress detection is also shown on specimens with an Invar core. The original image processing procedure has been developed to improve edge detection of obtained stress maps. The acoustic images are compared with theoretically predicted isocline contours. The inherent material anisotropy and the structural inhomogeneities influence significantly the acoustoelastic measurements. Advantages and limitations of the nondestructive technique are summarized on the basis of presented experimental results. © 2002 Elsevier Science B.V. All rights reserved.

Keywords: Acoustoelasticity; Birefringence; Residual stresses; Pulse acoustic microscopy

1. Introduction

The birefringence of shear acoustic waves (by the stress-induced anisotropy) is utilized for evaluation of plane stress in a plate specimen. In anisotropic media, the velocities of transversal waves depend on their polarization [1]. The conical polarized shear wave is generated in the plate by the defocused spherical acoustical lens. The corresponding echo reflected from the bottom surface of the specimen consists of elementary shear plane waves with a given polarization. Due to anisotropy, the elementary waves propagate with various velocities, and the amplitude of the resulting echo is sensitive to relative time delays among the elementary wave arrivals. Using this method, a precise measurement of the echo arrival time is replaced by the amplitude detection. The resulting acoustic image is formed by variations of the echo amplitude during mechanical scanning by the acoustical lens. This technique, using pulse acoustic microscopy, has been suggested and developed by Drescher-Krasicka [2,3].

The lens transforms the initial plane longitudinal wave to an aspherically focused wave in immersion (distilled water). This wave refracts on the specimen surface "1". The reflected longitudinal wave (L1L) from the surface "1" arrives at the lens. The transmitted longitudinal and transversal waves propagate into the material. The anisotropy induced by a plane pre-stress causes a splitting of the shear wave into waves marked as T and t with respect to the direction of the principal stress σ_1, σ_2. The velocities of wave propagation in the specimen are sensitive to the pre-stress state. Furthermore, the waves reflect on the bottom specimen surface "2", then transmit through the surface "1". The fundamental arriving waves are superimposed on the time separable wave packages **L**, **LL**, **LT**, **TT**, etc. as it is schematically shown in Fig. 1. In that figure, T $\Longleftrightarrow$ t wave conversion during reflection is also possible. The waveform **L** contains only the wave L1L, while the **LL**

* Corresponding author. Tel.: +4202-6605-3672; fax: +4202-858-4695.

E-mail address: ml@it.cas.cz (M. Landa).

PII: S0041-624X(02)00180-4

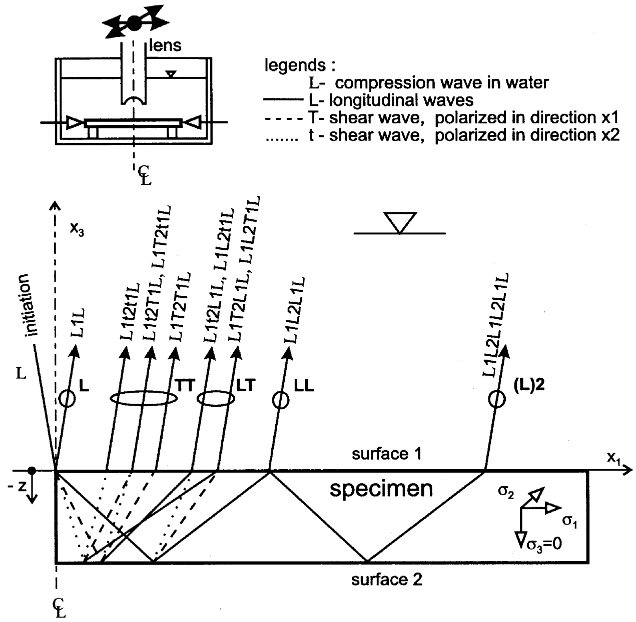

Fig. 1. Ray diagram of a spherical wave refraction in a pre-stressed specimen.

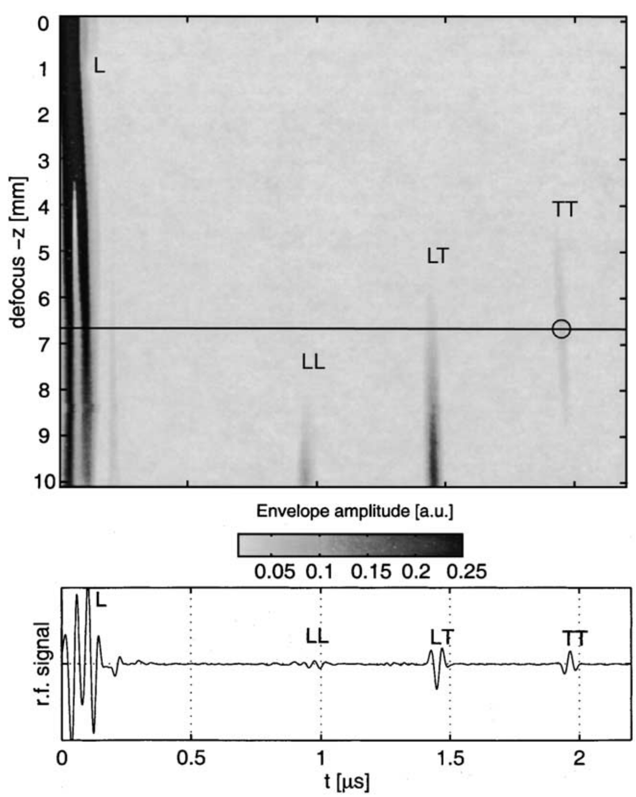

Fig. 2. Identification of the resulting echos in the image $V(z,t)$ and finding the optimal defocus distance z_o, for which the r.f. signal is plotted.

wave is a simple reflection from the surface "2". The **LT** wave package consists of the following converted waves tL, Lt, LT, TL. Finally, the **TT** represents the arrival of the pure shear waves TT, Tt, tT and tt. The other arriving wave (**L**)**2** is the L-wave reflected twice from the surface "1", which may appear in a surrounding of the echo **TT**. Due to the aspherical shape of the initial wave, the wavelets **LT** and **TT** represent integral response of the conical shear wave coming back to the interface "1". The fundamental waves cannot be distinguished, since they are superimposed onto the resulting echo. However, the echo amplitude is sensitive to relative time differences of the fundamental wave arrivals. The amplitude also depends on the defocus distance adjustment. The amplitude dependence $V(z,t)$ on the defocusing distance z and on the time delay t is shown in Fig. 2. The optimal defocus is marked by a line, and the echo **TT** is denoted by a circle. The resulting acoustic image is formed by amplitude variations of the echo **TT** during mechanical scanning by the acoustical lens.

For simplicity, the surface waves are omitted in the above ray analysis. The leaky surface waves are not expected for the following experimental conditions: 30 MHz transducer, an acoustical lens having a small apperture angle (13°), and a large focus distance (19 mm), the used range of defocusing distances z (from 0 to -10 mm, Fig. 2).

2. Specimens

The disks, 3 mm thick and 30 mm in diameter, were prepared from an unidirectional rolled bar and a plate (AlCu4BiPb), and also, from a multi-axial rolled semi-product (AlMg3). The elastic properties were measured on prismatic specimens by means of the pulse-echo contact method during compression tests, [4]. The first material shows hexagonal symmetry with respect to the rolling direction. Changes in the wave velocity of the second material in a stress free state were smaller than 0.3% with varying wave propagation direction. The full disks and the disks with the central hole (3 mm in diameter) were compressed with respect to the rolling direction. These disks, presented in Fig. 3a, were disks with the thermal stress introduced in them by heating them to 200 °C and inserting a cool Invar (Fe–Ni alloy) rod 6 mm in diameter with a 15 μm interference and were allowed to cool.

The isoclines (isolines of applied principal stress differences), induced in the disk by compression force $P = 5$ kN, were computed. These are plotted in Fig. 3b, where the scale of the stress differences is from 100 to 190 MPa. Since the isotropic material is considered, the computed principal stresses are independent of the elastic constants.

In the case of the Invar core forced into the Al disk, the principal stress difference $\Delta\sigma$ decays with the squared distance from the disk center and so the isoclines have a shape of concentric circles.

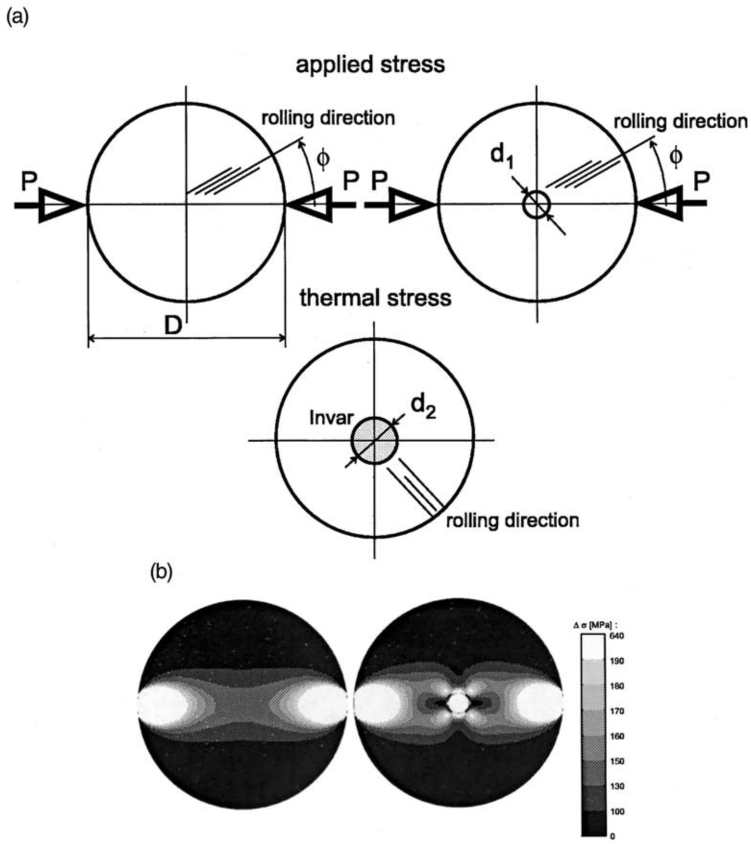

Fig. 3. (a) Specimen types, dimensions and loading scheme (thickness $h = 3$ mm, diameters: $D = 30$ mm, $d_1 = 3$ mm, $d_2 = 6$ mm). (b) Numerical (FEM) computation of "isoclines" in the circular disks (isotropic case) with a realistic distribution of the compression force ($P = 5$ kN).

3. Experimental arrangement

A special mechanical test machine with displacement and force control has been designed for in situ acoustoelastic measurements, using the pulse acoustic microscope Olympus UHPulse100 [4]. The commercial immersion transducer Panametrics V375 was utilized for the presented experiments. This equipment enabled the detection of both the positive (Ap) and negative (Am) amplitude of a time-delimitated echo. The resulting amplitude "V", forming acoustical images, was compounded as a sum $\mathrm{ADD} = Ap + Am$ or as a difference $\mathrm{SUB} = Ap - Am$. The optimal defocus distance $z_o = -6.60$ mm was determined from its dependence $V(z,t)$ on the defocus distance z and on time t (Fig. 2). For this defocus distance, the actual echos were identified from the r.f. signal in a time domain. The peak of the **TT**-echo was the subject of the analysis.

4. Image processing

Both images "ADD" and "SUB" were obtained in the form of 640×480 bit maps with 8 bits gray scale. The complete image post-processing was carried out using by Image Processing Toolbox at MATLAB. Both image speckle and noise were suppressed by double pass 2-D adaptive noise-removal filtering. The procedure is demonstrated on the acoustical images of the applied stress in the full disk ($AlCu_4BiPb$) loaded in the rolling direction by compression force $P = 4.93$ kN, Fig. 4.

The conventional approach to image sharpening (edge enhancement) is based on subtracting a multiple Laplacian around a pixel ($f(x,y) = g(x,y) - \mathrm{const.}\ \nabla^2 g(x,y)$), [5]. Our new approach utilized complementary character of "ADD" and "SUB" pictures. The enhanced image was arranged in the color channels of red, green and blue, using "ADD" and "SUB" maps in the following order: [R,G,B] = [255-SUB,ADD,255-SUB]. The other contrast enhancement, in terms of an individual image, was performed by using histogram equalization. In the end, the final contour plot was compared with the theoretical prediction (Fig. 3b). The resulting plot was calibrated, based on the assumption that there was a linear relation between the stress difference and the contours. For example, the expected value of $\Delta\sigma$ in the central point of the full disk is 141 MPa.

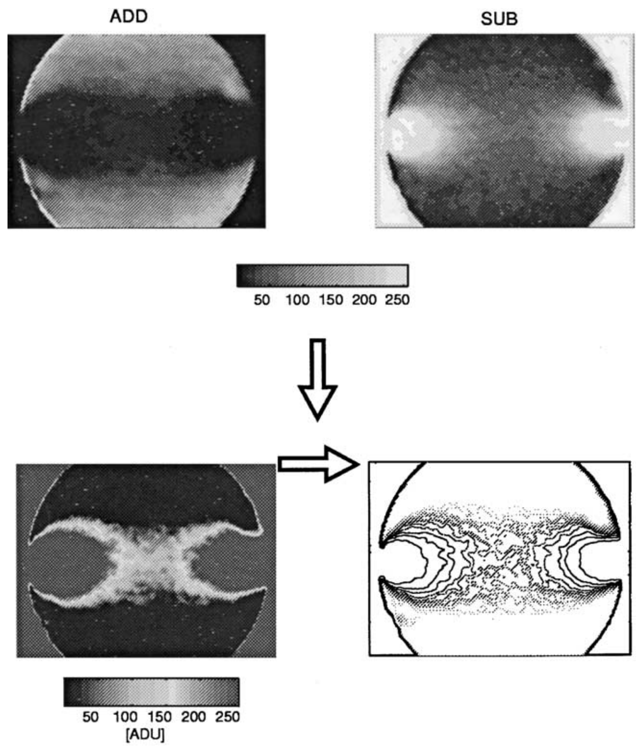

Fig. 4. Stress field maps ("ADD" and "SUB" amplitude mode detection) obtain on the full (AlCu4BiPb) disk, loading by the force $P = 4.93$ kN and sequential image processing.

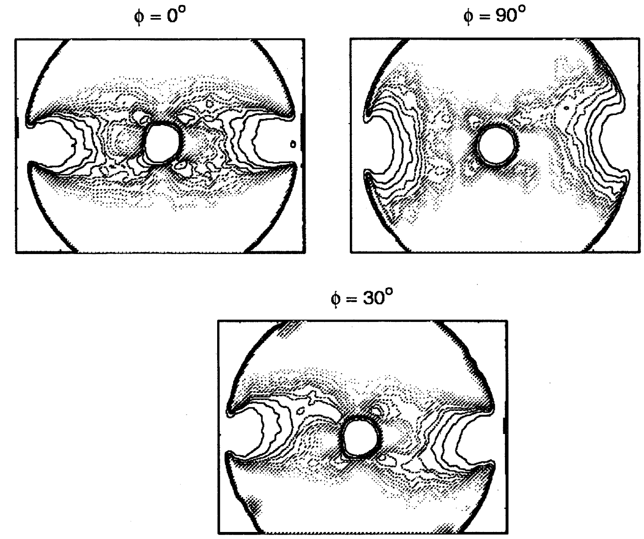

Fig. 5. Influence of the initial material anisotropy (AlCu4BiPb). The resulting stress contour changes with respect to angle ϕ between the loading and rolling direction. Applied force is 5 kN.

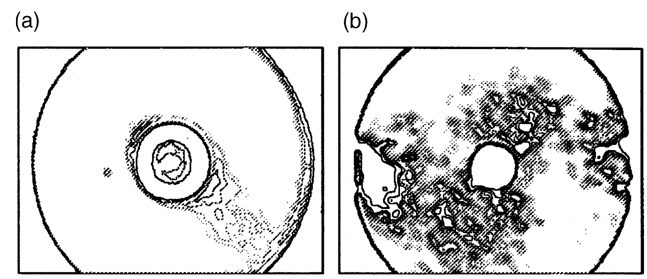

Fig. 6. (a) Internal stresses introduced by Invar core forced on; the orientation of contours coincides with the material anisotropy (AlCu4BiPb). (b) Influence of rough material structure (AlMg3); distortion of the contour plot due to wave scattering on inhomogeneities.

5. Analysis of results

The acoustical images of the specimens made from alloy AlCu4BiPb with dominant grain orientation due to sheet rolling were analyzed. The reversibility of applied stress in the elasticity range was observed [4]. The minimal value of the principal stress difference detectable by this technique was about 100 MPa.

The stress field detected around the central hole is presented in Fig. 5. For $\phi = 0°$ the evaluated contours have a shape close to the predicted isoclines, Fig. 3b, where is also shown the influence of loading direction ϕ changes with respect to the rolling direction. This is evident from the images for values $\phi = 30°$ and 90°. Anisotropy of the second-order elastic constants is too weak to have any importance in the computation of the static pre-stress within a range of numerical errors (Fig. 3b). Nevertheless, anisotropy in both the linear and nonlinear part of elasticity has the proportional influence on the wave propagation in pre-deformed media, and so a material texture orientation distort stress isoclines detected by acoustoelastic techniques. The same results are also mentioned in [6].

The visualisation of the residual stresses, induced by thermal expansion of the Al-alloy, is demonstrated on the specimen with Invar core (Fig. 6a). The specimen was free of applied stress, and its surfaces were undeformed. The stress field did not have the expected axial symmetry. The acoustoelastic effect was notable, but the resulting stress maps were also distorted by the dominant material texture.

The acoustical image of the loaded AlMg3 disk with the central hole is shown in Fig. 6b. The AlMg3 alloy was multi-axially rolled and could be considered as isotropic even for acoustoelastic measurement [4]. On the other hand, the mechanical and thermal treatments were the cause of the rough material structure and higher density of porosity. Acoustic waves scattered on the material inhomogeneities, and the resulting image lost information about the stress field.

The microstructure analysis of both materials $AlCu_4BiPb$ and AlMg3 confirmed the interpretation [4].

6. Concluding remarks

The technique, based on acoustoelastic birefringence and pulse acoustic microscopy, was utilized for the detection of either applied stress or thermal stress around stress concentrators in the disk specimen made from Al alloys. The contrast enhancement procedure was suggested and tested. The contours corresponding to the differences of the principal stress components, were identified.

The defocusing of the acoustical lens was necessary for the initiation of the shear waves propagation in the material. However, the lateral resolution of imaging, and thus the detectibility of the great stress gradient, was restricted by this defocusing.

Preferred grain orientation by rolling causes initial material anisotropy which distorts the detected stress contours. Elimination of the anisotropy feature from the evaluated stress contours is a difficult task. The problem is too complex to utilize an analytical approach. Application of a numerical approach for modeling of the acousto-stress interaction in the case of an inhomogeneous stress field in a material having anisotropy is very problematic. Acoustoelasticity is a weak effect, which is in direct proportion to numerical errors.

If the roughen grain structure and porosity appeared, the resulting stress image was destroyed by wave scattering. The presented method seems to be appropriate for residual stress evaluation at fine grain isotropic materials as in e.g. compact ceramics.

Acknowledgements

The authors wish to express their thanks to Ing. V. Očenášek, CSc. (VUK Panenské Břežany) for preparing alloys. This work has been supported by the Czech Grant Agency under the Post-doc. project no. 106/00/D106 and the project no. 101/99/0834.

References

[1] Y.H. Pao, W. Sachse, H. Fukuoka, in: W.P. Mason, R.N. Thurson (Eds.), Physical Acoustics, vol. 17, Academic Press, New York, 1984, pp. 61–120.
[2] E. Drescher-Krasicka, J. Acoust. Soc. Am. 94 (1993) 453.
[3] E. Drescher-Krasicka, J.R. Willis, Nature 384 (1996) 52.
[4] M. Landa, et al., Akustoelasticity II: Third order elastic constants, Internal stress mapping by means of acoustic microscopy (in Czech), Report No. Z1298/00, IT CAS, Prague, 2001.
[5] S.C. Wooh, TASME J. Eng. Mater. Technol. 112 (1990) 175.
[6] N.N. Hsu, Exp. Mech. 14 (1974) 169.